River Flow 2010 - Dittrich, Koll, Aberle & Geisenhainer (eds) - © 2010 Bundesanstalt für Wasserbau ISBN 978-3-939230-00-7

Overtopping and breaching of dikes – Breach profile and breach flow

L. Schmocker & W.H. Hager
Laboratory of Hydraulics, Hydrology and Glaciology VAW, ETH-Zurich, Zurich, Switzerland

ABSTRACT: Recent examples of dike breaching around the world (e.g. the Elbe flood in 2002, the New Orleans flood in 2005, or the Mississippi Flood in 2008) highlight the need for a detailed assessment of dike failure mechanisms, especially due to overtopping. Breaching of a dike can lead to extensive flooding of nearby areas along with both monetary and human losses. An accurate prediction of the dike failure process is essential to develop effective emergency action plans or establish adequate safety measurements. Therefore, systematic plane dike breach tests due to overtopping were conducted to understand the dike breach processes. All dikes were of trapezoidal shape, consisted of uniform non-cohesive sediment and were not protected by a core or a surface layer. The temporal dike breach progress was optically recorded to allow for a detailed analysis of the sediment and water flow surfaces. The tests resulted in basic findings regarding plane dike breach profiles. Further, a new equation for the discharge coefficient of the round-crested dike breach profile was obtained. The discharge during a dike breach can thus be determined depending on the breach profile radius and the angles of both the up- and downstream dike faces.

Keywords: Dike breaching; Flood; Hydraulic modeling; Risk management; Weir flow

1 INTRODUCTION

1.1 *Dike failure modes*

Dikes are earthen embankments to protect endangered regions and their population from seasonal floods. They are subjected to water loading for periods of only a few days or weeks a year and are therefore mostly constructed without a surface seal or a core. Compared to dams, dikes are short in height but can have lengths of several 100 km. Due to insufficient maintenance and increasing floods during the past years, dike breaching became a frequent cause of major flood events. For earth dikes in particular, the most common failure modes are (Singh 1996):

(1) Overtopping caused by extreme floods (hydraulic failure),
(2) Structural failure due to internal erosion or piping (hydraulic/geotechnical failure),
(3) Structural failure due to shear slide or foundation problems (geotechnical failure), and
(4) Failure due to natural or induced seismicity

As the majority of dikes breach due to overtopping, this failure mode was investigated in detail in the present investigation.

One of the first large studies on the mechanics of overflow erosion on embankments was conducted by Powledge et al. (1989 a, b). They presented various hydraulic aspects of dike overtopping along with a detailed discussion of the three main hydraulic and erosion zones, namely: (1) subcritical flow from the reservoir to the dike crest; (2) transcritical flow on the crest zone; and (3) rapidly-accelerating supercritical flow on the downstream dike slope. Coleman et al. (2002) conducted model studies on the overtopping failure of homogenous embankments of noncohesive sediment. Observations relative to the breach profile, the breach development and the breach discharge are presented.

A series of field tests to study the stability of embankment dams of various materials was presented by Höeg et al. (2004). The tests included failures due to overtopping and piping of up to 6 m high dams made of homogenous rockfill, clay or gravel. Between 2001 and 2004, the European IMPACT project provided valuable field and laboratory data to assess and develop breach models. The project highlights are summarized in a special issue of the Journal of Hydraulic Research (Garcia and Zech, 2007). In 2004, the integrated FLOODsite project was initiated with the objective to better assess and manage flood risks in Europe, including a state-of-the-art review on breach modelling (Morris 2008).

1.2 *Breach development*

Studies in the past investigated the breach development due to overtopping. An overview on spatial breach formation can be found in e.g. Singh (1996), Coleman et al. (2002), Visser at al. (2006), Rozov (2003), and Morris et al. (2008). The present investigation focuses only on the plane dike breach process. Powledge et al. (1989b) described the breach development for both granular and cohesive embankments due to overtopping. Erosion of granular embankments starts when the shearing stresses induced by the water flow over the downstream dike face exceed the critical shear stress of the dike material or the dike protection system made up by e.g. grass, gabions, geoweb or soil cement. Chinnarasri et al. (2003) observed four stages in plane dike erosion, namely: (1) Small erosion on dike crest after initial overtopping; (2) Slope sliding failure with ongoing erosion; (3) Wavelike-shaped dike profile; and (4) Large sediment wedge with small slope at erosion end. Similar processes were as well noted by Dupont et al. (2007), Wu and Wang (2008), and Schmocker and Hager (2009).

Cohesive embankments are generally more resistant to erosion than granular (Powledge et al. 1989b), mainly due to higher erosion resistance and lack of seepage as a result of the low permeability. Erosion often starts at the downstream embankment toe propagating from there upstream. The undercutting of the downstream slope removes large parts of material by shear failure on the over-steepened slope. In the present study, the development of the breach profiles was investigated for granular material and plane overflow erosion.

1.3 *Breach discharge*

For the plane dike erosion process presented herein, the discharge over the dike crest can be predicted using the general overflow formula

$$Q = C_d b\left(2gH_o^{\,3}\right)^{1/2} \tag{1}$$

with Q = overflow discharge, C_d = discharge coefficient, b = overflow width, g = gravitational acceleration, $H_o = h_o+Q^2/[2gb^2(h_o+w)^2]$ = energy head, h_o = overflow depth, and w = dike height. Herein, the discharge coefficient is mainly a function of the dike breach profile. Given the plane dike erosion process, the dike breach profile varies with ongoing erosion time (Fig. 1). After initial overtopping, the dike breach profile is similar to a broad-crested weir and C_D can be determined according to Fritz and Hager (1998) as

$$C_d = 0.43 + 0.06\sin\left[\pi\left(\xi - 0.55\right)\right] \tag{2}$$

with $\xi = H_o/(H_o + L_K)$ = relative crest length and L_K = crest length. With ongoing erosion, the dike breach profile gets more and more rounded (Fig. 1b, c), similar to a circular-crested weir. The discharge coefficient can be estimated using the standard circular-crested weir formula as

$$C_d = \frac{2}{3\sqrt{3}}\left(1+\frac{3\rho_k}{11+\Omega\rho_k}\right) \tag{3}$$

with $\rho_k = H_o/R$ = relative crest curvature, R = crest radius and $\Omega = 4.5$ (Hager 1994). However, C_d does not include the effect of the up- and downstream slopes of the breach profile. Especially the downstream dike slope varies strongly during a dike breach in the current investigation. Therefore, the effects of both the up- and downstream slopes on the discharge coefficient were investigated. The discharge coefficient was determined for a series of fixed, characteristic dike breach profiles.

The effect of sloping faces of a circular-crested weir has been studied by Ramamurthy and Vo (1993). For broad ranges of H_o/R, they tested upstream angles of 60°, 75°and 90°, and downstream slopes of 45°, 60°, and 75°. The upstream slope was found to have no effect on the discharge coefficient for a fixed downstream slope. For a fixed upstream slope, they observed an increase of the discharge coefficient for increasing downstream slopes. However, a specific equation for the discharge coefficient, including the effect of both side slopes, is still missing. In addition, the dike slopes in the present experiments are always below 45°.

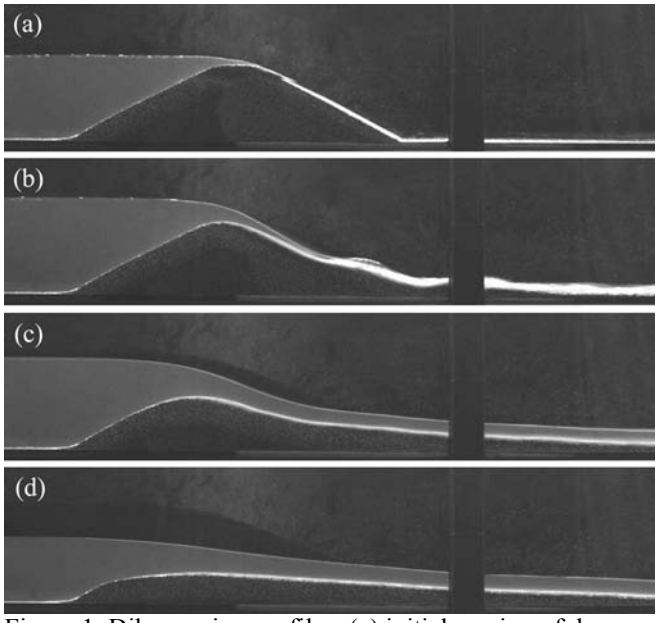

Figure 1. Dike erosion profiles: (a) initial erosion of downstream dike crest; broad-crested breach profile (b,c) circular-crested breach profiles and (d) equilibrium stage with large wedge breach profile

2 EXPERIMENTAL SETUP

2.1 *Hydraulic Model* 1 – *Dike erosion process*

The plane dike erosion tests were conducted in the rectangular VAW dike breach channel. The channel is 8 m long, 0.40 m wide, 0.70 m high, has a discharge capacity of $Q = 70$ l/s and its bottom is horizontal. The channel is considered hydraulic smooth and a flow straightener at its intake generated undisturbed inflow. The channel width was adjusted with PVC insets to $b = 0.20$ m. All dikes were inserted 1.0 m from the channel intake and the origin of the plane coordinate system (x, z) was located at the upstream dike toe (Fig. 2).

All dikes were of trapezoidal shape, consisted of homogenous, non-cohesive material and did not exhibit any surface protection or core. The seepage through the dike was controlled with a bottom drainage (Schmocker and Hager 2009). The following parameters were kept constant for all tests:

Dike height $w = 0.20$ m
Dike width $b = 0.20$ m
Crest length $L_K = 0.10$ m
Sediment: $d = 2.0$ mm, $\rho \approx 2{,}650$ kg/m^3
Dike slope $S_o = 1{:}2$ (V:H).
Dike length $L_D = 0.90$ m

A total of nine different tests were considered, with steady inflow discharges of $Q_o = 1$, 2, 4, 6, 8, 10, 12, 16, 20 l/s. The dike overflow was always free and the tailwater did not affect the basic erosion process. The discharge overtopped the dike on its entire width resulting in plane dike erosion. The streamwise dike profile observed through the channel side glass wall was therefore representative for the entire dike width. Small three dimensional erosion patterns, e.g. lateral deviations from the average erosion surface, were only observed after long erosion times. The breaching duration from initial overtopping to almost the equilibrium erosion profile was always about 500 s. Given this short breach duration and relatively small upstream reservoir, no constant reservoir level was attained. The tests can therefore only be applied to dike breach processes with a falling reservoir level.

The entire erosion process was filmed through the channel side wall, using a 30 Hz CCD camera. Both the water and sediment surfaces were directly derived from the camera records.

Major scale effects are absent for the chosen dike dimension and sediment size such that the effect of channel side wall can be neglected (Schmocker and Hager 2009). Regarding the approach flow discharges $Q_o = 1$ and 2 l/s, scale effects may occur as the breach flow is below fully turbulent flow. However, the effect on the general dike erosion process is small.

2.2 *Hydraulic Model* 2 – *Discharge coefficient*

The effect of the dike slopes on the discharge coefficient was investigated in a rectangular, horizontal channel at VAW. Its discharge capacity is 150 l/s, it is 0.50 m wide, 0.70m high and 7.0 m long, and its bottom is horizontal. The flow uniformity was improved with a flow straightener. Discharges up to 60 l/s were determined with a standard V-notch weir (±0.1%) and up to 120 l/s with Inductive Discharge Measurement (IDM). The overflow depth was measured with a point gage of ±0.2 mm reading accuracy.

Figure 3 shows the experimental setup for free overflow conditions, with h_o = overflow depth measured from the crest elevation, Q_o = discharge, R = crest radius, α_o = upstream (subscript o) angle, α_u = downstream (subscript u) angle, b = channel width and H_o = total overflow head. Circular-crested dike models made of steel were placed 3.5 m from the channel intake (Fig. 3). Two crest radii of $R = 0.15$ m and $R = 0.30$ m were tested and both the up- and downstream angle ranged from 20°, 30°, 45° to 90°. Ten combinations of up- and downstream angles were considered (Table 1). The standard circular-crested weir was tested using

$\alpha_o = \alpha_u = 90°$. For each dike profile, four different overflow depths were considered, namely $h_o = 0.05$, 0.10, 0.15 and 0.20 m for $R = 0.30$ m and $h_o = 0.075$, 0.10, 0.15 and 0.20 m for $R = 0.15$ m. For each dike profile and overflow depth, the inflow discharge Q_o was measured with either the V-notch weir or the MID. The discharge coefficient was then determined using Eq. (1) and compared with Eq. (3). Twenty dike profiles combined with four overflow depths resulted in a total of 80 measured discharge coefficients.

Table 1. Tested circular-crested dike breach profiles with various up- and downstream angles

	$R = 0.3$ m		$R = 0.15$ m	
Symbol	α_o [°]	α_u [°]	α_o [°]	α_u [°]
+	90*	90	90	90
⊠	90	45	90	45
□	90	30	90	30
⊞	90	20	90	20
▽	45	90	45	90
△	30	90	30	90
×	20	90	20	90
◇	20	30	20	30
○	30	30	30	30
◺	20	20	20	20

* no side slopes
(Symbols used in Fig. 9)

3 OBSERVATIONS AND PRELIMENARY RESULTS

3.1 *Erosion Profiles*

During each test both the water surface $h(x,t)$ and the sediment surface $z(x,t)$ with t = time were recorded using a 30 Hz CCD camera of a resolution of 1,034(H)× 778(V) pixels, resulting in a accuracy of ±0.015w for both profiles. The sediment surface $z(x,t)$ was then directly derived from the camera records. Figure 4 shows the particular dike erosion profiles $X(Z)$ with $X = x / L_D$ and $Z = z / w$ at various times for $Q_o = 10$ l/s. Overtopping starts at $t = 0$ s, with the dike still in its original shape. The initial erosion then starts at the downstream dike crest. The minor sediment accumulation at $X = 0.85$ at $t = 2$ s results from the small overflow discharge transporting sediment downwards. The water front consisted of a sediment-water mixture, similar to a debris flow. At $t = 4$ s, the erosion advances fast and the dike crest is already rounded. The eroded material forms a small mound at $X = 1.25$ but is already washed away at $t = 6$ s due to the increased breach flow. At $t = 15$ s, the dike has reduced to half of its original height. The eroded material forms a large tailwater wedge. The erosion advances and finally leaves an almost stable 'equilibrium' dike surface. During the erosion process, both the crest radius and the downstream dike slope increase significantly with the upstream slope remaining at 1:2. This erosion process was observed for all tested discharges.

The dike overflow is related to the discharge over an embankment, as indicated by Powledge et al. (1989b). The flow condition upstream of the dike is subcritical. Transitional flow occurs on the dike crest and the flow on the downstream slope is supercritical. The hydraulic control point is located at the highest instantaneous dike elevation. The velocity increases significantly over the downstream dike slope such that the tractive shear stresses result in high erosion. As the energy head and the tractive shear stresses decrease as the dike crest height reduces, the erosion both at and beyond the original dike crest slows down.

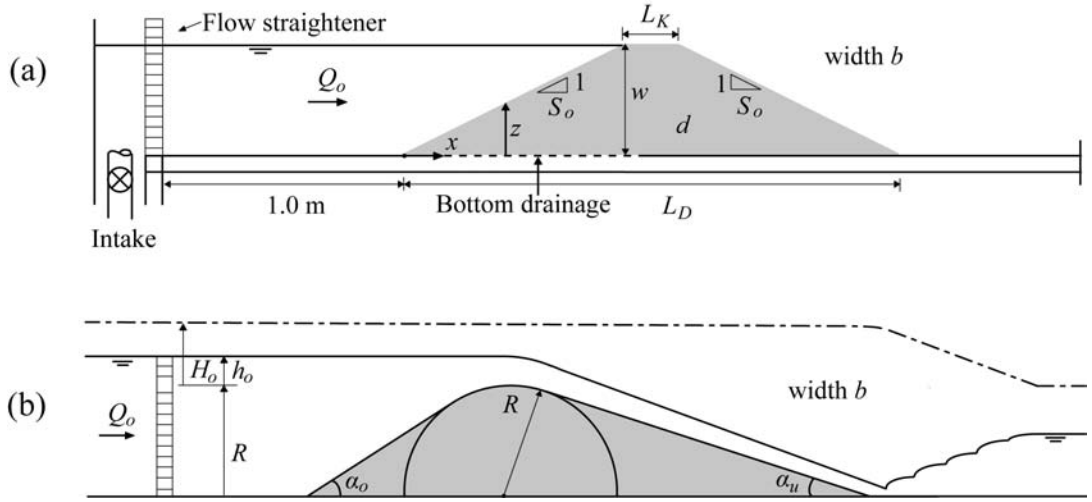

Figure 2. (a) Hydraulic model 1: Streamwise section of VAW plane dike breach model and (b) Hydraulic model 2: Definition of flow geometry for free overflow over representative dike erosion profile, notation

Sliding of the downstream dike face was only observed for Q_o = 1 and 2 l/s. The bottom drainage was not efficient enough for theses small discharges. Due to the long reservoir filling times, the seepage line reached the downstream dike face before overtopping started. The water drained from the dike body and eroded the downstream dike toe similar to a piping failure. This resulted in backward erosion of the downstream dike face (Fig. 5). The eroded dike face was still stable, yet with a smaller slope S. However, the effect of sliding failure on the entire breach process is comparatively small, as discussed below.

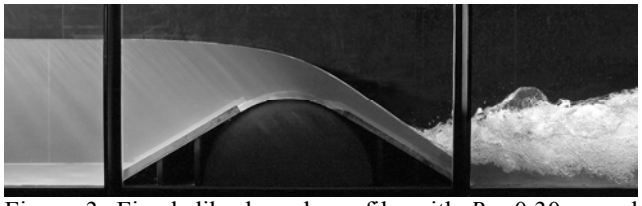

Figure 3. Fixed dike breach profile with R = 0.30 m and $\alpha_o = \alpha_u$ = 30 °.

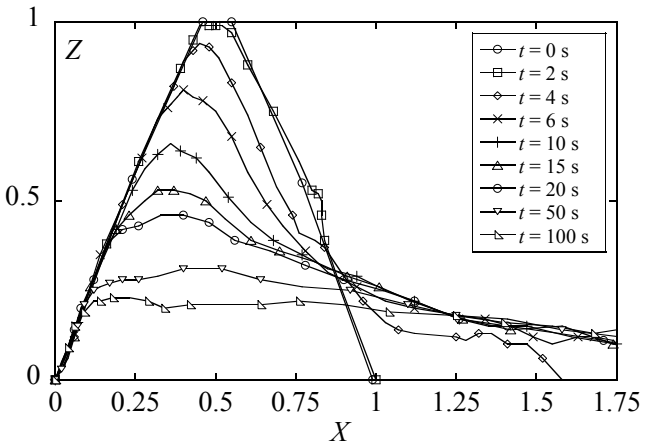

Figure 4. Dike breach profiles $Z(X)$ at various times t for Q_o = 10 l/s, w = 0.20 m, b = 0.20 m, L_K = 0.10 m and d = 2.00 mm

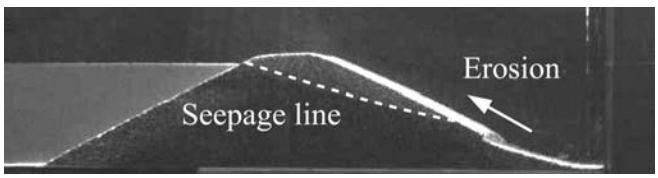

Figure 5. Backward erosion due to seepage for Q = 1.0 l/s, b = 0.20 m, w = 0.20 m, L_K = 0.10 m and d = 2.0 mm

3.2 *Maximum dike height*

The maximum (subscript m) dike height $z_m(t)$ during the erosion process was derived for all tested discharges. Figure 6 shows the normalized maximum dike elevation $(1–Z_m)(t)$ with $Z_m = z_m/w$. For all tested discharges, Z_m decreases fast after initial overtopping and then gradually slows down as both the dike height and the tractive shear stress decrease. For all tests, the maximum dike height reaches eventually the equilibrium (subscript e) height $Z_{me} = z_{me}/w$ after a certain time t_e. For Q_o = 1 l/s, the equilibrium dike height is $Z_{me} \approx 0.43$ at t_e = 200 s. For Q_o = 20 l/s, the dike is eroded completely (Z_{me} = 0) at t_e = 600 s. The maximum equilibrium dike height Z_{me} follows from Fig. 7 as

$$\left(1 - Z_{me}\right) = 0.64 + 0.019 Q_o \qquad (4)$$

for 1 l/s $\le Q_o \le$ 20 l/s. For Q_o < 1 l/s, $Z_{me} \to 1$, whereas for Q_o > 20 l/s, Z_{me} = 0. Eq. (4) is limited to the present experiments and data set, as it is dimensionally incorrect. A detailed analysis is required to account for a dimensionless interpretation of the results. Therefore, no direct application or up-scaling to prototype dimensions is currently possible.

For each discharge Q_o and time t, the maximum dike heights Z_m were normalized with Z_{me} as $\zeta = (1–Z_m)/(1–Z_{me})$. Figure 8 shows $\zeta(t)$ for all tests. All data collapse on a single curve as

$$\zeta = \tanh\left(\frac{t}{140}\right)^{0.2} \qquad (5)$$

The general dike erosion process is therefore similar for all test discharges. The normalized maximum dike height decreases linearly with t for small erosion times, then advances slowly and reaches the equilibrium state. The largest deviation are seen for Q_o = 1 l/s. Small overflow depths result in Reynolds numbers $\mathrm{R} = 4V \cdot R_h/\nu < 10^5$, with R_h = hydraulic radius and ν = kinematic fluid viscosity, i.e. below fully-turbulent flow. The erosion potential is therefore too small as compared to the higher discharges. In addition, the observed sliding failure prior to initial overtopping leads to a smaller downstream dike slope and therefore a decreased flow velocity. The effect on the entire erosion process is however surprisingly small. Again, Eq. (5) is dimensionally incorrect as it only applies to the present data set.

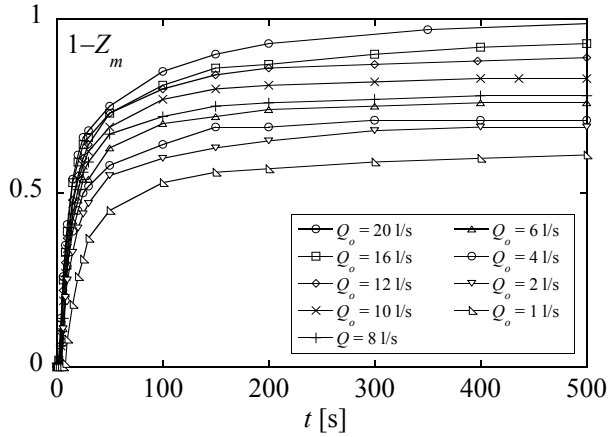

Figure 6. Maximum dike height $(1–Z_M)$ versus breach time t for all tested discharges

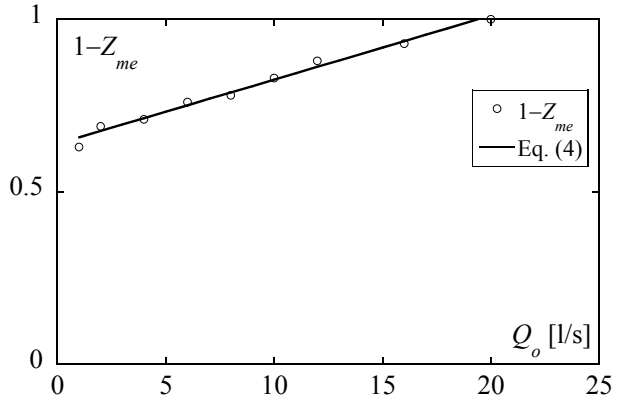

Figure 7. Maximum equilibrium dike height $Z_{me}(Q_o)$ for all tested discharges with (–) Eq. (4)

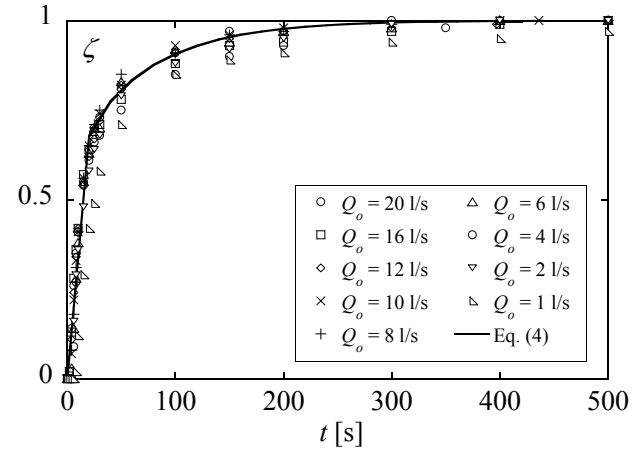

Figure 8. Normalized maximum dike height $\zeta(t)$ for all tested discharges compared with (–) Eq. (5)

3.3 *Discharge coefficient*

The discharge coefficient was investigated using fixed dike erosion profiles (2.2) with various radii and up- and downstream slopes. For each tested profile, the discharge coefficient was determined with Eq. (1) using the discharge Q_o and the corresponding energy head H_o. The values of $C_d(\rho_k)$ were afterwards compared with Eq. (3) for the standard circular-crested weir. It was found that C_d for such a weir with up- and downstream slopes is generally lower as compared with the standard circular-crested weir (Halldórsdóttir 2009).

The data indicate that for fixed values of ρ_k and α_u, C_d does not significantly change with α_o. This is in agreement with previous studies e.g. Ramamurthy and Vo (1993). The upstream slope contributes to the streamlining of the weir flow and tends to increase C_d. However, it although adds to the upstream area over which the flow occurs, therefore decreasing C_d. The data for both fixed ρ_k and α_u and variable downstream angles α_u indicate that C_d decreases as the downstream slope reduces. This effect becomes more apparent for increased ρ_k. The discharge coefficient is always smallest for $\alpha_u = 20°$. A steeper downstream angle improves the weir performance, increasing the overflow discharge for a fixed overflow depth (Halldórsdóttir 2009).

To account for the embankment angles of circular-crested weirs, all C_d values were normalized using the dimensionless parameter

$$\rho_k' = \frac{H_o}{R}\left(\frac{\alpha_o + 2\alpha_u}{270}\right)^{\frac{1}{3}} \tag{4}$$

with H_o/R = relative crest curvature and $[(\alpha_o+2\alpha_u)/270]^{1/3}$ = embankment angle ratio parameter. As the effect of the downstream angle is predominant, it is multiplied with two, resulting in the best data fit. For the standard circular-crested weir with vertical sides ($\alpha_o=\alpha_u=90°$), the second parameter equals 1, and $\rho' = \rho = H_o/R$. The discharge coefficient may be expressed according to Hager 1994 with ρ_k' instead of ρ_k as

$$C_d = \frac{2}{3\sqrt{3}}\left(1 + \frac{3\rho_k'}{11 + \Omega\rho_k'}\right) \tag{5}$$

with $\Omega = 4.5$. Figure 9 shows $C_D(\rho_k')$ for all tests and Eq. (5) with $r^2 = 0.98$. The angle ratio parameter increases the data fit significantly and Eq. (5) can therefore be used to determine the coefficient of discharge for circular-crested weirs with arbitrary up- and downstream angles.

3.4 *Breach discharge*

The breach flow can be calculated using Eqs. (1), (4) and (5) for each time step of dike erosion. The profile radius, both the up- and downstream angles and the overflow depth were directly derived from the camera records. Figure 10 shows the breach discharge hydrograph $Q(t)$ for the approach flow discharge $Q_o = 4$ l/s.

As soon as overtopping starts, Q increases fast and reaches its maximum of $Q_m \approx 7.4$ l/s at $t \cong 10$ s. The breach discharge Q therefore exceeds Q_o, particularly if dike erosion is fast and the reservoir volume is emptied. After reaching the maximum outflow, the breach discharge decreases slowly until $Q = Q_o$. This feature was observed for all tested discharges. Currently, a detailed analysis of all test is conducted to account for normalized breach flow information.

4 OUTLOOK

The erosion profiles have so far been analyzed for one specific dike dimension and grain size along with various steady inflow discharges. The results are therefore limited to this test setup.

However, the results indicate that a detailed investigation of the plane dike breach problem is possible using the current hydraulic model. It allows to consider a wide range of test conditions with a comparatively small effort. Besides the variation of Q_o, the present tests conducted at VAW include: (1) Dike heights w = 0.15, 0.20, 0.30 m; (2) Sediment diameters d = 1, 1.5, 2, 4, 5.5 mm; and (3) Dike slopes S_o = 1:2, 1:2.5 and 1:3. The main goal is a detailed analysis of all these parameters regarding their effect on the plane dike erosion process. These results are of significance in applications presented in the Introduction of this work.

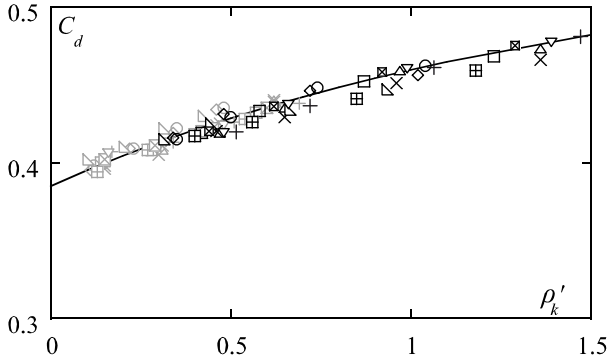

Figure 9. Measured normalized discharge coefficients $C_d(\rho_k')$ with (–) Eq. (5). R = 0.30 m (grey symbols) and R = 0.15 m (black symbols). Notation Table 1.

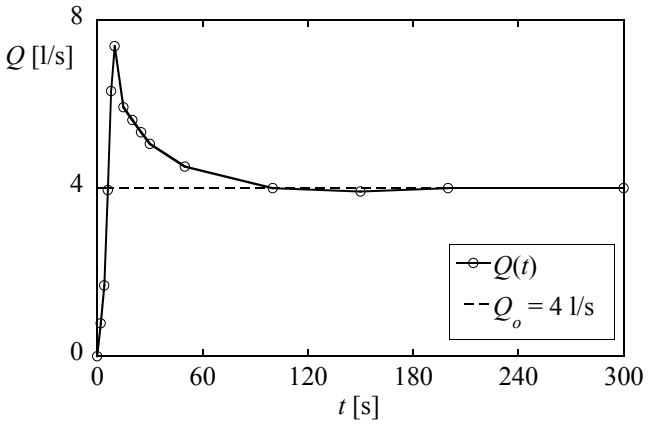

Figure 10. Breach discharge hydrograph $Q(t)$ for steady inflow discharge Q_o = 4 l/s

5 CONCLUSIONS

Systematic plane dike breach tests have been carried out using a simple model dike. The dike consisted of homogenous, non-cohesive material and did not exhibit any surface layer or core. A steady inflow scenario was tested, resulting in a falling reservoir level with ongoing erosion. The dike breach process was documented through the channel side wall using a CCD camera.

The observed dike erosion profiles are similar to those observed in the literature. The dike develops from its original trapezoidal shape to a rounded profile, similar to a circular-crested weir with both up- and downstream slopes, and finally forms a large tailwater wedge. The erosion process was described using the maximum dike elevation. The major part of the erosion occurs shortly after initial overtopping with the energy level in the reservoir still at its maximum. An almost equilibrium dike profile is attained toward erosion end. However, additional tests have to be conducted to account for all major factors affecting the dike breach process. Especially the erosion time has to be analysed more systematically.

The discharge coefficient for the rounded breach profile with various up- and downstream slopes was investigated using fixed dike breach profiles. The results indicate the effect of the dike radius and especially the downstream embankment angle on the discharge. A generalized equation for the discharge coefficient of circular-crested weirs with various up- and downstream angles is also presented.

ACKNOWLEDGMENTS

The authors would like to thank Miss Berglind Rósa Halldórsdóttir for her laboratory assistance.

The first writer was supported by the Swiss National Science Foundation, Grant No. 200020-116680.

REFERENCES

Chinnarasri, C., Tingsanchali, T., Weesakul, S., Wongwises, S. 2003. Flow patterns and damage of dike overtopping. Intl. Journal of Sediment Research 18(4), 301-309.

Coleman, S.E., Andrews, D.P., Webby, M.G. 2002. Overtopping breaching of noncohesive homogeneous embankments. Journal of Hydraulic Engineering 128(9), 829-838.

Dupont, E., Dewals, B.J., Archambeau, P., Erpicum, S., Pirotton, M. 2007. Experimental and numerical study of the breaching of an embankment dam. Proc. 32nd Congress of IAHR Venice 1(178), 1-10. IAHR, Madrid.

Fritz, H.M., Hager, W.H. 1998. Hydraulics of embankment weirs. Journal Hydraulic Engng. 124(9), 963-971.

Garcia, M.H., Zech, Y., eds. 2007. Dam-break flow experiments and real-case data: A database from the European IMPACT research program. Journal of Hydraulic Research 45, Extra Issue.

Hager, W.H. 1994. Discussion of 'Momentum model for flow past weir', by Ramamurthy, A.S., Vo., N.-D., Vera, G. Journal of Irrigation and Drainage Engineering 120(3), 684-685.

Halldórsdóttir, B.R. 2009. Hydraulics of dike overflow. Master Thesis. VAW, ETH Zurich, Zurich.

Höeg, K., Lövoll, A., Vaskinn, K.A. 2004. Stability and breaching of embankment dams: Field tests on 6 m high dams. Hydropower & Dams 11(1), 88-92.

Morris, M.W. 2008. *Breaching processes*: A state-of-the-art review. European Commission FLOODsite report T06-06-03, Contract No.GOCO-CT-2004-505420 (www.floodsite.net).

Morris, M.W., Hassan, M.A.A.M., Samuels, P.G., Ghataora, G.S. 2008. Development of the HR BREACH model for predicting breach growth through flood embankments and embankment dams. Proc. Intl. Conf. River Flow, Çeşme, Turkey, 679-687.

Powledge, G.R., Ralston, D.C., Miller, P., Chen, Y.H., Cloppner, P.E., Temple, D.M. 1989a. Mechanics of overflow erosion on embankments 1: Research activities. Journal of Hydraulic Engineering 115(8), 1040-1055.

Powledge, G.R., Ralston, D.C., Miller, P., Chen, Y.H., Cloppner, P.E., Temple, D.M. 1989b. Mechanics of overflow erosion on embankments 2: Hydraulic and design considerations. Journal of Hydraulic Engineering 115(8), 1056-1075.

Ramamurthy, A.S., Vo, N.-D. 1993. Characteristics of circular crested weir. Journal of Hydraulic Engineering 119(9), 1055-1062.

Rozov, A.L. 2003. Modeling of washout of dams. Journal of Hydraulic Research 41(6), 565-577.

Schmocker, L., Hager, W.H. 2009. Modelling dike breaching due to overtopping. Journal of Hydraulic Research, 47(5), 585-597.

Singh, V.P. 1996. Dam breach modelling technology. Kluwer, Dordrecht.

Visser, P.J., Zhu, Y., Vrijling, J.K. 2006. Breaching of dikes. Proc. 30th Intl. Conf. Coastal Engng., San Diego CA, 2893-2905.

Wu, W., Wang, S.S.Y. 2008. One-dimensional explicit finite-volume model for sediment transport with transient flows over movable beds. Journal Hydraulic Res. 46(1), 87-98.